doi:10.1016/j.jmb.2009.02.054 J. Mol. Biol. (2009) 388, 195–206

JMB

Available online at www.sciencedirect.com

ScienceDirect

ELSEVIER

Threshold Occupancy and Specific Cation Binding Modes in the Hammerhead Ribozyme Active Site are Required for Active Conformation

Tai-Sung Lee[1,2], George M. Giambaşu[1,2], Carlos P. Sosa[1,3], Monika Martick[4], William G. Scott[4] and Darrin M. York[1,2]*

[1]*Biomedical Informatics and Computational Biology, University of Minnesota, Minneapolis, MN 55455, USA*

[2]*Department of Chemistry, University of Minnesota, 207 Pleasant Street SE, Minneapolis, MN 55455, USA*

[3]*Blue Gene Software Development, IBM, Rochester, MN 55901, USA*

[4]*Department of Chemistry and Biochemistry and the Center for the Molecular Biology of RNA, Sinsheimer Laboratories, University of California at Santa Cruz, Santa Cruz, CA 95064, USA*

Received 30 September 2008; received in revised form 17 February 2009; accepted 23 February 2009
Available online 2 March 2009

Edited by D. Case

The relationship between formation of active in-line attack conformations and monovalent (Na^+) and divalent (Mg^{2+}) metal ion binding in hammerhead ribozyme (HHR) has been explored with molecular dynamics simulations. To stabilize repulsions between negatively charged groups, different requirements of the threshold occupancy of metal ions were observed in the reactant and activated precursor states both in the presence and in the absence of a Mg^{2+} in the active site. Specific bridging coordination patterns of the ions are correlated with the formation of active in-line attack conformations and can be accommodated in both cases. Furthermore, simulation results suggest that the HHR folds to form an electronegative recruiting pocket that attracts high local concentrations of positive charge. The present simulations help to reconcile experiments that probe the metal ion sensitivity of HHR catalysis and support the supposition that Mg^{2+}, in addition to stabilizing active conformations, plays a specific chemical role in catalysis.

Keywords: RNA; simulations; ion distribution; in-line conformation; hammerhead RNA

Introduction

It remains an open question how RNA molecules can catalyze a broad range of reactions with efficiency that rivals those of many protein enzymes, with fairly limited chemical functional groups available from the sugar phosphate backbone and four relatively inert nucleobases.[1] One hypothesis is that RNA enzymes (*ribozymes*) may recruit metal ions and other solvent components to facilitate catalysis through electrostatic engineering. In the case of the hammerhead ribozyme (HHR),[2] it is generally accepted that, under physiological conditions, divalent metal ions are required for the chemical steps of catalysis. Recent crystallographic studies of a full-length HHR have characterized the ground-state active-site architecture[3] and solvent structure,[4] including the binding mode of a presumed catalytic divalent metal ion in the active site, and have reconciled a long-standing controversy between structural and biochemical studies for this system.[5] Based on these new crystal structures, molecular simulations studies[6,7] have suggested a role for the divalent metal ion in the chemical reaction. From these simulations, it has been proposed that the di-

*Corresponding author. Department of Chemistry, University of Minnesota, 207 Pleasant Street SE, Minneapolis, MN 55455, USA. E-mail address: york@umn.edu.

Abbreviation used: HHR, hammerhead ribozyme.

valent metal ion can serve to stabilize active in-line conformations and interact with key residues to facilitate acid/base catalysis. Further studies have explained the origin of mutational effects on catalysis.[8] Nonetheless, it is known that, under high nonphysiological salt concentrations, the HHR and other ribozymes remain catalytically proficient,[9–11] bringing into question the extent to which divalent metal ion occupancy in the active site is strictly necessary or just a sufficient condition to achieve efficient catalysis that might be affected by other cations and solvent components.

The modeling of ions in highly charged systems such as RNA affords tremendous challenges with regard to simulation time scales. The reason is that the equilibration and sampling times of mass transport/diffusion-limited processes (such as ion migration) and subsequent macromolecular structural relaxation are notoriously slow.[12] In the present study, we report the results of a series of five 300-ns simulations of the full-length HHR, in both the reactant ground state and the activated precursor state, in order to explore the relationship between cation binding modes and active in-line conformation. Results indicate that the HHR has an electronegative cation recruiting pocket in the active site that, upon threshold occupancy, stabilizes catalytically active in-line attack conformations via specific cation binding patterns. These results provide a first glimpse into a possible common feature that might be exploited by other ribozymes: the engineering of electrostatically preorganized active sites that are able to recruit solvent components to facilitate catalysis.

Results and Discussion

Simulations performed

A recent joint crystallographic/molecular simulation study[4] of the solvent structure of the full-length HHR indicates that an Mn^{2+} is coordinated with the O_{2P} atom of the A9 phosphate and the N7 atom of G10.1. This binding site is designated as the "C-site." An alternate binding site where a divalent metal ion bridges A9:O_{2P} and the scissile phosphate (C1.1:O_{2P}), designated as the "B-site," has been inferred from thio/rescue effects[13,14] and also predicted from molecular simulations.[6,7] In the absence of divalent metal ions, HHR activity can be recovered by high concentrations of monovalent ions.[9–11] The specific metal ion binding modes at different stages along the HHR reaction coordinate and their relation to the formation of catalytically active structures have not yet been determined. The present work reports the results of a series of molecular dynamics simulations aimed at providing atomic-level insight into these questions.

To explore the divalent and monovalent metal ion binding modes (Fig. 1) and their relation to the formation of catalytically active in-line attack conformations in both the neutral reactant state and the activated precursor state (deprotonated 2′OH nucleophile), we set up the following series of simulations (summarized in Table 1):

1. RT-C-Mg: the reactant state with Mg^{2+} at the C-site
2. RT-B-Mg: the reactant state with Mg^{2+} at the bridging position
3. dRT-C-Mg: the activated precursor with Mg^{2+} initially placed at the C-site
4. dRT-B-Mg: the activated precursor with Mg^{2+} at the bridging position
5. RT-Na: the reactant state in the absence of Mg^{2+} (in the presence only of NaCl)
6. dRT-Na: the activated precursor in the absence of Mg^{2+} (in the presence only of NaCl).

dRT-C-Mg simulation, an activated precursor with Mg^{2+} initially placed at the C-site, quickly (less than 200 ps) led to migration of the Mg^{2+} into the B-site position, as observed in a previous simulation study,[7] and afterward exhibited a nearly identical behavior as if the Mg^{2+} was initially placed at the B-site (dRT-B-Mg). Hence, we only extended the dRT-B-Mg simulation to 300 ns and designated it simply as dRT-Mg.

All five simulations have been extended to 300 ns in a background of 0.14 M NaCl. The equilibration of each simulation was monitored by RMSD and had reached steady states after 30–50 ns (see Supplementary Data). Hence, all analyses were performed over the last 250 ns of trajectories for each simulation.

Threshold occupancy and specific coordination patterns of ions are highly correlated with catalytically active conformations

To understand the relationship between active in-line conformation and metal ion binding patterns, we first examine metal occupation and coordination numbers in the active site. Four key coordination sites are used for characterizing metal binding (Fig. 1): G8:$O_{2'}$, A9:O_{2P}, C1.1:O_{2P}, and C17:$O_{2'}$. The averages, denoted by $\langle\rangle$, of the following three quantities were calculated for both Mg^{2+} and Na^{+}: N is the number of ions with at least one coordination with any one of the four key coordination sites, CN is the total coordination number of ions with at least one coordination with any one of coordination sites, and BN is the number of ions that coordinate with at least two of the four coordination sites.

Active conformation can be examined by the distribution of nucleophile in-line attack angle and distance. Their distributions from all simulations are shown in Fig. 2 and manifest two *k*-mean clusters:[16] cluster A (red) containing structures in near-in-line attack conformations, and cluster B (blue) containing structures not in near-in-line attack conformations, with the exception of the dRT-Mg simulation, where only cluster A is found.

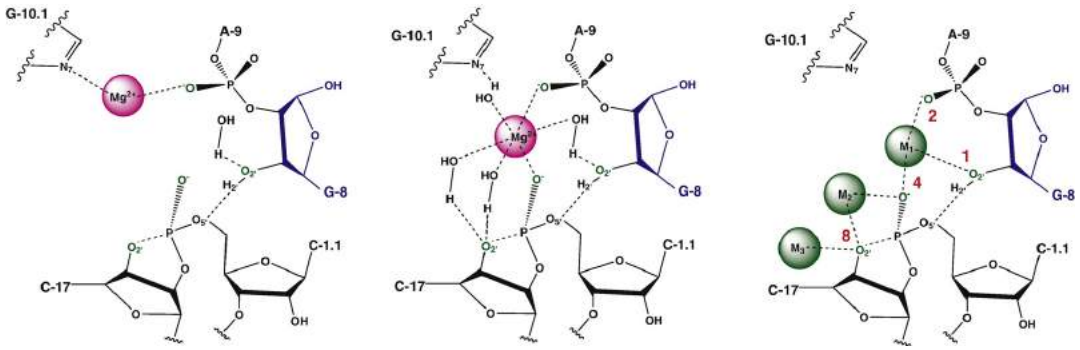

Fig. 1. Schematic view of the coordination sites in the HHR active site. Left: The coordination pattern of Mg^{2+} in the "C-site" coordinated with G10.1:N_7 and A9:O_{2P}. Middle: The coordination pattern of Mg^{2+} in the "B-site" bridging A9:O_{2P} and C1.1:O_{2P} of the scissile phosphate. Right: Coordination sites for Na^{+} in the HHR active site found in the RT-Na and dRT-Na simulations. Red numbers next to the coordination sites are the scores used to calculate the coordination index (see the text). M_1 involves direct binding to A9:O_{2P} and C.1:O_{2P} and indirect binding to G10.1:N_7 through a water molecule. M_2 involves direct binding to C17:$O_{2'}$ and C.1:O_{2P}. M_3 involves direct binding to C17:$O_{2'}$ and is positioned toward the outside of the active site.

Table 1. Index of simulations

Abbreviation	State of 2′OH	Mg^{2+}	[NaCl] (M)	Temperature (K); pressure (atm)	Simulation (ns)	Analysis (ns)
RT-C-Mg	Neutral reactant	C-site	0.14	298; 1	300	250
RT-B-Mg	Neutral reactant	B-site	0.14	298; 1	300	250
dRT-C-Mg	Deprotonated precursor	C-site	0.14	298; 1	<1	—
dRT-B-Mg/dRT-Mg	Deprotonated precursor	B-site	0.14	298; 1	300	250
RT-Na	Neutral reactant	Absent	0.14	298; 1	300	250
dRT-Na	Deprotonated precursor	Absent	0.14	298; 1	300	250

Each simulation is given an abbreviation referenced in the text. The simulations differed in the protonation state of the 2′OH nucleophile (state of 2′OH), being either in the "neutral reactant" or in the "deprotonated precursor" state. The simulations also differed from the presence/absence and initial placement of the Mg^{2+} in the active site. In the presence of a Mg^{2+} in the active site, initial placement could be in the "C-site" coordinated with O_{2P} of the A9 phosphate and N7 of G10.1, or in the "B-site" position bridging between the O_{2P} atoms of the A9 and scissile phosphates. In the "dRT-C-Mg" simulation of the deprotonated precursor with Mg^{2+} initially placed in the C-site, the Mg^{2+} quickly migrated to a B-site position and exhibited dynamics essentially equivalent to the dRT-B-Mg simulation, and thus was not carried out further or analyzed. All simulations were carried out in 0.14 M NaCl at 298 K and 1 atm and, with the exception of the "dRT-C-Mg" simulation mentioned above, were carried out to 300 ns, the last 250 ns of which was used for analysis.

Metal occupation and coordination numbers were then analyzed for each cluster, and the results are listed in Table 2. During all simulations, when present in the active site, one Mg^{2+} remained stably bound at full occupancy ($\langle N_{Mg^{2+}} \rangle = 1.00$). In the reactant-state simulations RT-C-Mg and RT-B-Mg, there is no significant population of Na^+ in the active site ($\langle N_{Na^+} \rangle \leq 0.1$), which suggests that the Mg^{2+} is sufficient to neutralize the local charge of the A9 and scissile phosphates. In the RT-C-Mg (Mg^{2+} at the C-site) simulation, the Mg^{2+} directly coordinates only A9:O_{2P} of the RNA ($\langle CN_{Mg^{2+}} \rangle = 1.00$) and thus is not involved in a bridge ($\langle NB_{Mg^{2+}} \rangle = 0.00$). Cluster A (in-line conformation) represents approximately 21% of the sampled data over the last 250 ns of simulation, whereas cluster B (not in-line conformation) represents the remaining 79%.

The RT-B-Mg (Mg^{2+} at the bridging position) simulation, on the other hand, is dramatically different. In this simulation, the Mg^{2+} directly coordinates both A9:O_{2P} and the scissile phosphate C1.1:O_{2P} of the RNA ($\langle CN_{Mg^{2+}} \rangle = 2.00$) as a stable bridge ($\langle NB_{Mg^{2+}} \rangle = 1.00$). Cluster A, containing a high degree of in-line near-attack conformations, represents the vast majority of the sampled data (over 99%), whereas cluster B is observed less than 1% of the time. This suggests that a bridging Mg^{2+} contributes to stabilization of catalytically active conformations in reactant simulations.

This feature is even more pronounced in the dRT-Mg simulation (activated precursor state with Mg^{2+}). There is only a single cluster with in-line conformation ($\theta = 155°$). For dRT-Mg, an additional negative charge in the active site arises from deprotonation of the nucleophile, and a single Na^+ is observed in the active site ($\langle N_{Na^+} \rangle = 0.97$), making direct coordination with only one RNA ligand ($\langle CN_{Na^+} \rangle = 1.01$) with essentially no bridging interactions.

On the other hand, the simulations without an active-site Mg^{2+} are considerably different from those with the divalent ion present. In the reactant RT-Na simulation, cluster A is dominant (87% of the time) and shows a high degree of in-line conformations ($\theta = 153°$). Most of the cluster A population contains a single Na^+ in the active site ($\langle N_{Na^+} \rangle = 1.15$), less frequently two Na^+ ions, and the average number of bridging Na^+ is 0.88. Cluster B, on the other hand, has a slightly higher active-site Na^+ occupation ($\langle N_{Na^+} \rangle = 1.38$), but a lower average number of bridging ions (0.66).

In the activated precursor dRT-Na simulation, the average Na^+ occupancy ($\langle N_{Na^+} \rangle$) increases to approximately 3 and 2.5 for clusters A and B, respectively. Cluster B (not in-line conformation) is the dominant population, occurring 76% of the time. Cluster A (in-line conformation) occurs 24% of the time.

A striking feature that distinguishes cluster A from cluster B is that the former exhibits a very high degree of bridging ion character, in addition to higher Na^+ occupancy. For cluster A, the average number of these ions that coordinate at least two RNA ligands ($\langle NB_{Na^+} \rangle$) is 2.68, while the number is only 1.36 for cluster B.

These results suggest that the bridging coordination patterns are highly correlated with the formation of in-line conformations for both cases with and without Mg^{2+}. Besides the above ion occupation and coordination number analysis, we further look into the specific binding patterns for both cases with and without the Mg^{2+}.

Bridging Mg^{2+} maintains rigid coordination patterns that stabilize in-line attack conformations

In this section, we compare the effect of different Mg^{2+} binding modes in both neutral reactant and activated (deprotonated 2′OH) precursor states on active-site structure and fluctuations. Table 3 lists the averages of key in-line indexes, the A9/scissile phosphate–phosphate distance, and Mg^{2+} coordination distances for RT-C-Mg, RT-B-Mg, and dRT-Mg simulations. Figure 1 shows a general schematic view of the active-site metal ion coordination from the simulations. The distances and standard deviations indicate that the Mg^{2+} retains rigid coordination with phosphate oxygens over the course of the

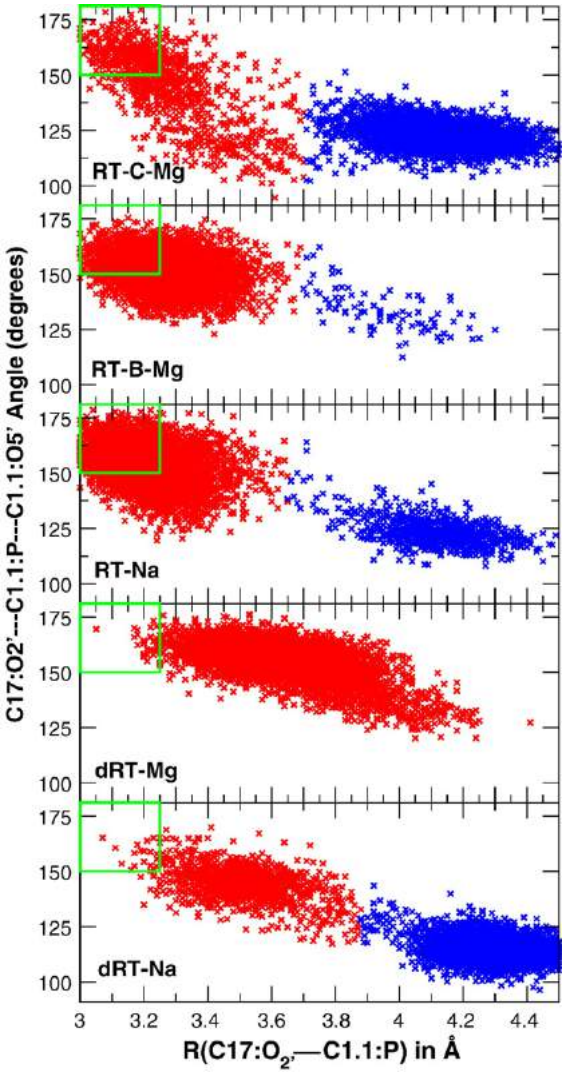

Fig. 2. Plot of the $O_{2'}$–P–$O_{5'}$ angle *versus* the $O_{2'}$–P distance for the approach of the 2′-hydroxyl of residue C17 to the phosphate of residue C1.1 for the reactant-state (RT) and the activated-state (dRT) simulations. C-Mg indicates that the Mg^{2+} was initially placed at the C-site position,[4] while B-Mg means the Mg^{2+} was initially placed in an equatorial bridging position.[6,7] Data obtained from the last 250 ns of the simulations are shown with a frequency of 50 ps, and points are colored according to the clustering results and Table 2: red, cluster A; blue, cluster B. Green lines at 3.25 Å and 150° indicate the near-in-line attack conformation (NAC) region defined by Torres and Bruice.[15]

simulation, being directly coordinated with A9:O_{2P} in all simulations. In the RT-C-Mg simulation, the Mg^{2+} coordinates G10.1:N_7 indirectly through one of four inner-sphere water molecules. However, this coordination pattern is not highly conducive to the formation of an in-line attack conformation. The RT-B-Mg simulation, on the other hand, shows a more rigid Mg^{2+} coordination with both A9 and scissile phosphate oxygens, and sustains a considerable population of in-line attack conformations. These results suggest that the coordination pattern found in the RT-B-Mg simulation is able to stabilize in-line attack conformations more readily than Mg^{2+} binding at the C-site, as in the RT-C-Mg simulation. The dRT-Mg simulation is similar to the RT-B-Mg simulation with regard to exhibiting rigid coordination with the A9 and scissile phosphate oxygens and stabilization of in-line attack conformations.

With the Mg^{2+} at the bridging position (RT-B-Mg and dRT-Mg simulations), there is considerably reduced interaction with G10.1:N_7, which is compensated for by interactions with the C17:$O_{2'}$ that occur through two water molecules in the inner sphere of the Mg^{2+}. This interaction is most pronounced in the dRT-Mg simulation where the C17:$O_{2'}$ is deprotonated. In the ground-state reactant simulations with Mg^{2+} (RT-C-Mg and RT-B-Mg), no Na^+ was observed to infiltrate the active site. In the activated precursor simulation dRT-Mg, a single Na^+ was observed to be bound at high occupancy to the deprotonated C17:$O_{2'}$ in a manner similar to the M_3 position in Fig. 1.

Na^+ ions bind nonspecifically and exhibit different coordination patterns in the reactant and activated precursor states

In this section, we explore the monovalent metal ion binding modes that are correlated with the formation of catalytically active in-line attack conformations. For the simulations with no Mg^{2+} (RT-Na and dRT-Na) in the active site, binding of the Na^+ to the coordination sites exhibits larger variations, and exchange events occur, giving rise to a fairly broad array of coordination patterns. In order to characterize the distribution and frequency of this array of coordination patterns, a binary-coded coordination index is used (Fig. 1). This index is defined as follows. When a Na^+ is within a cutoff distance (3.0 Å) to a ligand, it is classified as bound to the ligand and assigned a unique coordination score for binding to that particular ligand. The coordination scores for the four possible coordination sites (ligands) are 1 for G8:$O_{2'}$, 2 for A9:O_{2P}, 4 for C1.1:O_{2P}, and 8 for C17:$O_{2'}$. The coordination index of an ion is the sum of all coordination scores from its bound sites. In this way, the coordination pattern of a Na^+ can be uniquely represented by a single number. For example, an index of 12 means that a Na^+ directly coordinates with both C1.1:O_{2P} and C17:$O_{2'}$ simultaneously (4+8=12). Through this coordination index, the coordination patterns of Na^+ in the active site can be traced as a time series over the course of the simulation, as shown in Fig. 3. Distinct colors are also used to distinguish individual Na^+ present in the active site such that transitions between coordination patterns (indexes) can be monitored.

Figure 3 shows that in the RT-Na simulation, two Na^+ ions (in red and green) are present in the active site and, most of time, they both have a coordination index of 6, indicating binding to both A9:O_{2P} and C1.1:O_{2P} at the same time (2+4=6; refer to Fig. 1). Hence, two Na^+ ions collectively act like a single

Table 2. Coordination patterns of Mg^{2+} and Na^+ in the active site

	Cluster	Percentage	R^a	θ^b	$\langle N_{Mg^{2+}}\rangle^c$	$\langle CN_{Mg^{2+}}\rangle^d$	$\langle NB_{Mg^{2+}}\rangle^e$	$\langle N_{Na^+}\rangle^c$	$\langle CN_{Na^+}\rangle^d$	$\langle NB_{Na^+}\rangle^e$
RT-C-Mg	A	20.78	3.30	144.05	1.00	1.00	0.00	0.05	1.00	0.00
	B	79.22	4.13	122.66	1.00	1.00	0.00	0.03	1.00	0.00
RT-B-Mg	A	99.54	3.27	151.10	1.00	2.00	1.00	0.00	1.00	0.00
	B	0.46	4.00	129.76	1.00	2.00	1.00	0.09	1.00	0.00
RT-Na	A	86.72	3.23	152.91	—	—	—	1.15	1.99	0.88
	B	13.28	4.12	122.82	—	—	—	1.38	1.54	0.66
dRT-Mg	A	100.00	3.64	154.89	1.00	2.00	1.00	0.97	1.01	0.01
dRT-Na	A	23.99	3.50	144.72	—	—	—	2.96	2.29	2.68
	B	76.01	4.30	115.16	—	—	—	2.46	1.69	1.36

Distances and angles (Fig. 1) are in expressed in angstroms and degrees, respectively. The average values, denoted as ⟨⟩, are obtained by averaging over all snapshots in the cluster.
[a] R is the in-line attack distance (C17:$O_{2'}$ to C1.1:P).
[b] θ is the in-line attack angle (between C17:$O_{2'}$, C1.1:P, and C1.1:$O_{5'}$).
[c] N is the number of ions with at least one coordination with any one of the four coordination sites.
[d] CN is the total coordination number of all ions with at least one coordination with any one of the four coordination sites.
[e] NB is the number of ions that coordinate with at least two of the four coordination sites.

bridging Mg^{2+} to hold the negatively charged A9 and scissile phosphates together to maintain an in-line conformation. During the period from approximately 210 ns to 240 ns, only one Na^+ (red) with a coordination index of 6 is present in the active site. During this period, the in-line angle drops suddenly from around 155° to 120°. In those periods, the in-line conformation is no longer held.

In the dRT-Na simulation, the in-line angle is less well preserved than in the dRT-Mg simulation. This is consistent with the lower activity of the ribozyme in the absence of Mg^{2+}. Nonetheless, there are several periods (e.g., 25–50 ns and 210–270 ns) where an in-line conformation is visited, and again we observe a high correlation between the Na^+ coordination index and in-line conformation. When less than three Na^+ ions bind to the active-site ligands, the in-line conformation is no longer held, which happens during most of the simulation. During the periods of simulation, three Na^+ ions bind to different ligand sites simultaneously, and the in-line angle comes to a ready-to-react value (≥150°).

Figure 4 illustrates the different Na^+ binding patterns for cluster A (defined in Table 2, in-line conformation, lower panels) and cluster B (not in-line conformation, upper panels) from the dRT-Na simulation. The in-line cluster A clearly exhibits three Na^+ bridges that involve C17:$O_{2'}$/C1.1:O_{2P}, C1.1:O_{2P}/G8:$O_{2'}$, and C1.1:O_{2P}/A9:O_{2P}. On the other hand, for cluster B, the first two of these bridges are absent, with the third being significantly less pronounced.

The above analysis suggests that the compensation of the negative charges of these three coordination sites, as well as the bridging binding patterns of Na^+ to bring them together, is necessary to keep the in-line conformation in the deprotonated activated precursor state, although the binding patterns are not as rigid as those of Mg^{2+}.

The HHR active site forms a local electronegative recruiting pocket for cation occupation

In this section, we examine the preferential occupation of cations in the HHR active site. The three-dimensional density contour maps for the Na^+ distribution determined over the last 250 ns of simulation (Fig. 5) show that the Na^+ density at a medium contour level (Fig. 5, left) is located near the RNA's phosphate backbone, whereas at high contour level (Fig. 5, right), the highest probabilities of Na^+ occupation sites are all concentrated in the active site for both the reactant and the activated precursor. No explicit Na^+ was initially placed in the active site, and Na^+ exchange events were observed to occur. This suggests that the HHR folds to form a strong local electronegative pocket that attracts Mg^{2+} or Na^+. As analyzed by NMR, a similar case

Table 3. Characterization of Mg^{2+} coordination in the active site

	R^a	θ^b	O–O^c	A9:O_{2P}^{d}	C1.1:O_{2P}^{d}	C17:$O_{2'}$^{d}	G8:$O_{2'}$^{d}	G10:$N_{7'}$^{d}
RT-C-Mg	4.01 (34)	126.5 (119)	4.14 (49)	2.01 (4)	4.40 (30)	6.04 (90)	5.76 (46)	4.19 (31)
RT-B-Mg	3.28 (12)	151.2 (79)	2.95 (13)	2.02 (5)	2.04 (5)	4.25 (24)	4.57 (30)	4.38 (25)
dRT-Mg	3.64 (17)	155.0 (80)	2.94 (13)	2.01 (4)	2.03 (5)	3.76 (17)	4.62 (62)	5.05 (26)

Analysis was performed over the last 250 ns (sampling frequency, 10 ps). Distances and angles (Fig. 1) are in expressed in angstroms and degrees, respectively. Standard deviations are listed in parentheses divided by the decimal precision of the average (e.g., if the average is reported to two digits of decimal precision, the SD is divided by 0.01).
[a] In-line attack distance (C17:$O_{2'}$ to C1.1:P).
[b] In-line attack angle (between C17:$O_{2'}$, C1.1:P, and C1.1:$O_{5'}$).
[c] Distance between A9:O_{2P} and C1.1:O_{2P}.
[d] Distance between the Mg^{2+} and the indicated ligand site.

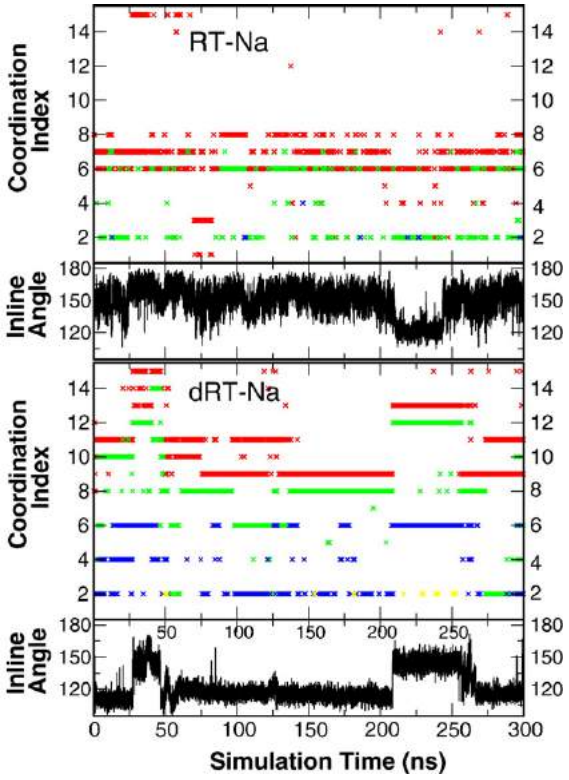

Fig. 3. Plot of the in-line attack angle ($O_{2'}$–P–$O_{5'}$; in degrees) and the coordination index of Na^+ for the RT-Na (top) and dRT-Na (bottom) simulations. The coordination index is defined as follows: when a Na^+ has a distance of less than a 3.0-Å cutoff value to a ligand, it is defined as bound to that ligand for indexing purposes. When an ion is bound, the scores for the four possible coordination sites are 1 for G8:$O_{2'}$, 2 for A9:O_{2P}, 4 for C1.1:O_{2P}, and 8 for C17:$O_{2'}$. The coordination index of a single Na^+ is the sum of all scores from its bound sites. Individual Na^+ ions are tracked using different colors (red, green, blue, and yellow). Data obtained from the last 250 ns are shown in steps of 500 ps.

has been observed in the tetraloop–receptor complex, where the divalent ions were experimentally found to be located at strong electronegative positions formed by the RNA fold.[17]

Together with the known divalent metal ion binding at the C-site, these results provoke the speculation that perhaps the active sites of some ribozymes such as the HHR have evolved to form electrostatic cation binding pockets that facilitate catalysis. In the case of the HHR, this speculation is further supported by the simulated correlation of cation binding mode with the formation of active conformations discussed in detail in previous sections.

Discussion

Our simulations suggest that in order to maintain the active in-line conformation, the highly negatively charged environment of the active site needs to be balanced by threshold cation occupancy. This can be accommodated in the reactant state by either a single Mg^{2+} or one to two Na^+ ions. In the activated precursor state, this is accomplished by a Mg^{2+} and an additional Na^+, or three Na^+ ions. Moreover, to form active in-line conformations, these ions must adopt specific bridging coordination patterns: either a bridging Mg^{2+} or specific patterns of bridging Na^+ ions.

It has been well established that, in the absence of divalent ions, the HHR retains activity at a high concentration of monovalent ions.[10] The properties of hammerhead cleavage in high concentrations of monovalent ions are similar to those in the presence of divalent metal ions, which has been interpreted as indicative of the major role of the cations in simple electrostatic stabilization of the phosphates, and allow folding into an active conformation. However, there remains some smaller contribution to the rate enhancement that can be effected through a more active role played by at least one divalent metal ion, as observed by rate reduction in the presence of only monovalent[9] or exchange inert ions.[11]

There are notable exceptions whereby hammerhead cleavage differed significantly in the presence and in the absence of divalent metal ions. Disruption of implicated divalent metal binding sites at G10.1:N_7, A9:O_{2P}, and C1.1:O_{2P} has significant deleterious effects on hammerhead cleavage in the presence of divalent ions, but not in high concentrations of Li^+. For example, both A9:O_{2P} and C1.1:O_{2P} exhibit significant catalytic thio effects that can be rescued by thiophilic ions such as Cd^{2+}. Moreover, both G10.1:N_7 and A9:O_{2P} form a divalent metal ion binding site, as pinpointed by electron spin-echo envelope modulation[18] and as observed crystallographically for the full-length HHR.[4] The present simulation results are consistent with those experimental evidence and indicate that threshold occupancy and specific coordination patterns of either Mg^{2+} or Na^+ can electrostatically stabilize the active site and facilitate active in-line conformations. These results provide detailed insight into the specific structural roles played by divalent and monovalent ions.

It has been demonstrated that the sensitivity of HHR activity to divalent ions is reduced upon introduction of tertiary stabilizing motifs.[19–23] A recent study of the tertiary stabilized RzB HHR has led to the suggestion that HHR catalysis may occur through a multichannel mechanism that has available both a divalent-dependent pathway and a divalent-independent pathway.[22] These experiments, together with previous measurements of pH–rate profiles,[21] are consistent with the interpretation that the divalent ion may play a specific nonstructural role in catalysis. The present simulation results provide insight into the nature of the different metal ion binding patterns that give rise to catalytically active conformations and further support the previous supposition that Mg^{2+}, in a bridging position, plays an active chemical role by interacting with the leaving group (C1.1:$O_{5'}$) and general acid (G8:$O_{2'}$).[7]

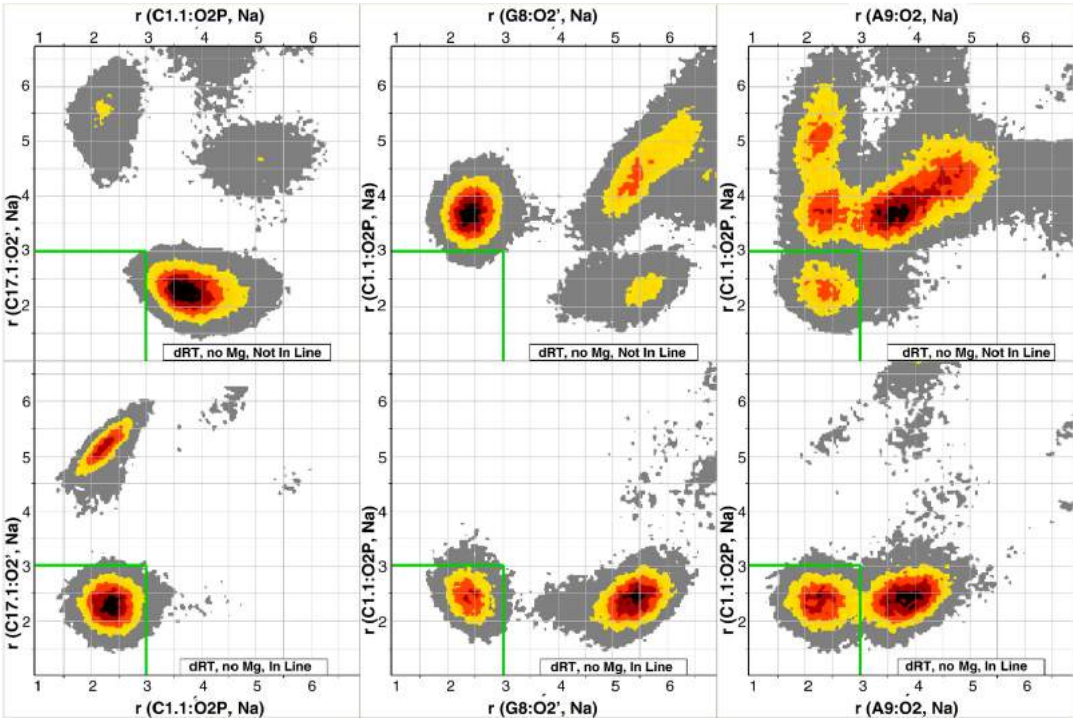

Fig. 4. Two-dimensional radial distribution function of Na^+ in the active site for the activated precursor simulation without Mg^{2+} present in the active site (dRT-Na). The lower panels show results for cluster A, which contains population members that are on active in-line conformations, and the upper panels show results for cluster B that are not on in-line conformation (see Table 2). Axes are the distances (in Å) to different metal coordination sites. Green lines indicate the regions where Na^+ ions have distances of less than 3.0 Å to both sites indicated by the axes.

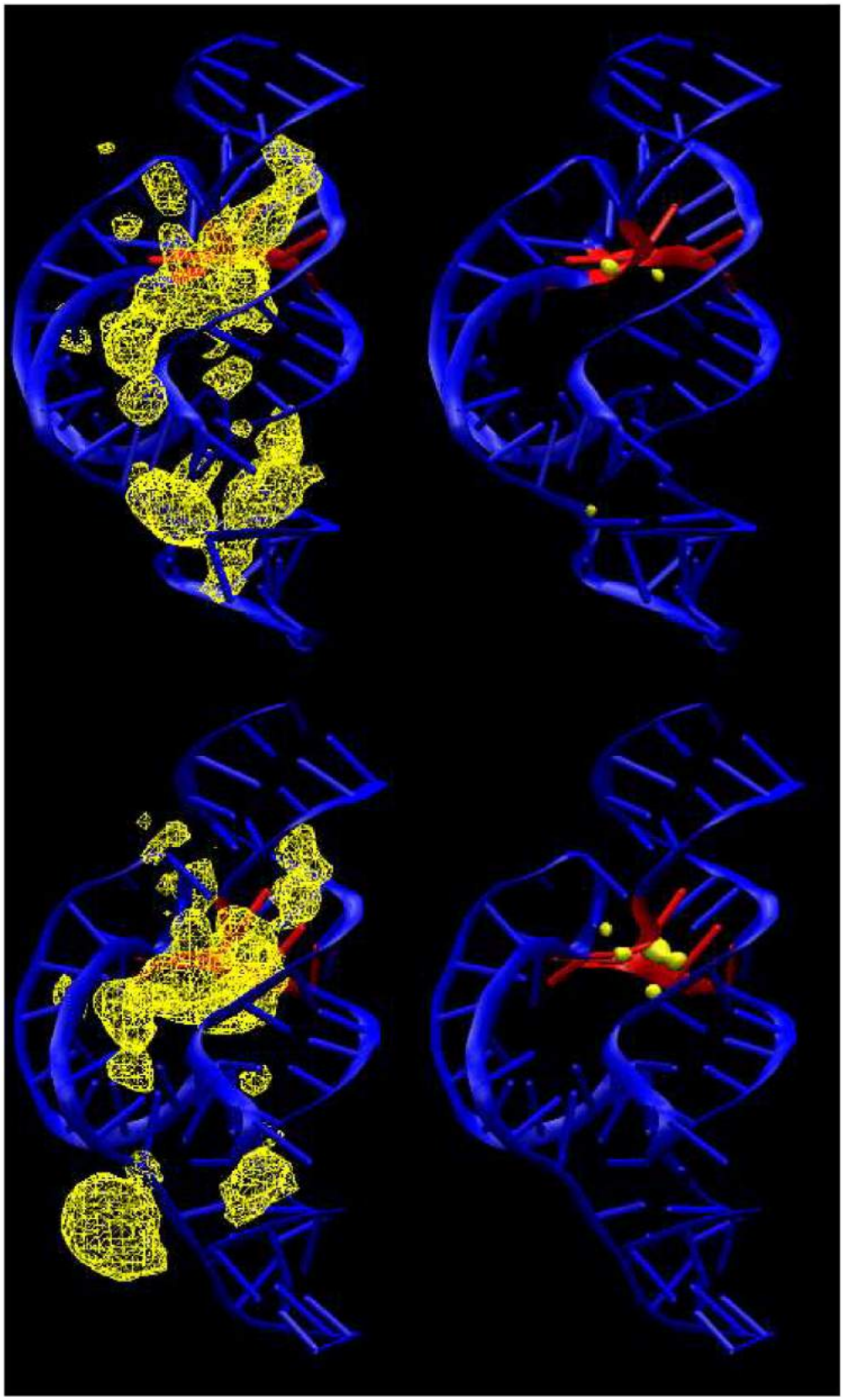

Fig. 5. The three-dimensional density contour maps (yellow) of Na^+ distributions derived from the RT-Na (upper panels) and dRT-Na (low panels) simulations at different isodensity contour levels (left: 0.1; right: 1.0). The HHR is shown in blue, with the active site highlighted in red. The figure shows that although the Na^+ ions distribute around the RNA phosphate backbone (left), the HHR folds to form a local electronegative recruiting pocket that attracts a highly condensed distribution of the Na^+ ions (left panels) both in the reactant state and in the deprotonated activated precursor state (deprotonated C17:$O_{2'}$) simulations.

The present study provides direct evidence for the involvement of threshold cation occupation in the active site and the formation of specific ion binding patterns as requirements for the formation of catalytically active conformations. The implications of these results support the hypothesis that ribozymes may exploit electrostatic engineering of the active site to recruit ions in order to facilitate catalysis. This does not imply that the recruitment of such ions is a necessary condition for catalysis, but is suggestive that it may be one successful strategy that ribozymes have evolved to exploit. In the case of other ribozymes such as the hairpin ribozyme, there has been recent evidence based on combined quantum mechanical/molecular mechanical simulations suggesting that the electrostatic environment of the active site alone may account for a considerable percentage of the observed rate enhancement without explicit involvement in metal ions.[24,25] That the pK_a values of implicated nucleobase functional groups may be shifted into the physiological pH range by electrostatic and ionic environments has recently been demonstrated for the *Neurospora* VS ribozyme.[26] The full extent to which ribozymes may use electrostatic organization, either directly or indirectly by establishment of a specific ionic environment, as a general strategy to facilitate catalysis remains an open question. An understanding of these and other general principles that govern ribozyme activity is a central goal that would enable the design of new RNA-based technology.

Materials and Methods

Initial structures used in the simulations were based on a 2.0-Å crystal structure with divalent Mn^{2+} and solvent resolved (Protein Data Bank 2OEU),[4] with Mn^{2+} replaced by native Mg^{2+} in the simulations. The positions of hydrogen atoms were determined using the VMD program (version 1.8.6).[27] Simulations were performed in a cubic cell (60 Å×60 Å×100 Å) filled with preequilibrated TIP3P[28] waters. The ion atmosphere consisted of Na^+ and Cl^- that were added to neutralize the system and to reach a concentration of 0.14 M. The resulting system contains 36,534 atoms: 11,463 water molecules, 5 Mg^{2+} ions, 83 Na^+ ions, 29 Cl^- ions, and 2021 RNA atoms.

Simulations were performed with the NAMD simulation package (version 2.6)[29] using the all-atom Cornell *et al.* force field (parm94)[30] in CHARMM format, provided in the AMBER 9 package.[31,32] Periodic boundary conditions were used along with the isothermal–isobaric ensemble (*NPT*) at 1 atm and 298 K, using extended system pressure algorithm[33] with an effective mass of 500.0 amu and using Nosé–Hoover thermostat[34,35] with an effective mass of 1000.0 kcal/mol ps^2, respectively. The smooth particle mesh Ewald method[36,37] was employed with a B-spline interpolation order of 6 with a κ value of 0.2579. Fast Fourier transform grid points of 60, 60, and 100 were used for the lattice directions x, y, and z, respectively. Nonbonded interactions were treated using an atom-based cutoff of 12 Å, with switching of nonbond potential beginning at 10 Å. Numerical integration was performed using the leap-frog Verlet algorithm with a 1-fs time step.[38] Covalent bond lengths involving hydrogen were constrained using the SHAKE algorithm.[39]

The following equilibration procedures (10 ns total) were applied to the system prior to the production simulations. The positions of the solute atoms, including the Mg^{2+}, were restrained by a harmonic potential of 50 kcal/mol/Å^2 in the equilibration stage.

Preannealing stage

Water and ion molecules were first energy-optimized for 2000 steps then underwent constant volume simulation annealing. The temperature was increased from 0 K to 298 K at a rate of 1 K/ps. The system then was kept at 298 K for 500 ps.

Solvent annealing stage

First, the temperature was increased from 298 K to 600 K at a rate of 1 K/ps, then it was kept at 600 K for 500 ps with constant volume. Second, the temperature decreased from 600 K to 298 K at a rate of 1 K/ps, then was kept at 298 K for 1500 ps with constant volume. Third, the system was kept at 298 K for 3000 ps at constant pressure (1 atm). The whole annealing stage was repeated twice before the postannealing stage.

Solute relaxation stage

After the annealing stage, the solute atoms were energy-optimized and then allowed to move under harmonic restraints over a 500-ps simulation at 298 K at a constant pressure of 1 atm. The harmonic force constant (in kcal/mol/Å^2) on each heavy atom was obtained from the empirical formula $k_i = 25 + 2\times10^3/B_i$, where k_i is the force constant for atom i and B_i is the corresponding crystallographic B-value. The restraints were exponentially released over 500 ps, with a half-life decay parameter of 100 ps. At the end of the 500-ps simulation, the restraints were reduced to about 3% of the initial restraint values.

Production simulation

After 10 ns of solvent equilibration, the whole system was energy-optimized, and unconstrained dynamics simulation began at 0 K under a constant pressure of 1 atm. The temperature was increased to 298 K at a rate of 1 K/ps and then kept fixed at 298 K. The same equilibration process was applied for each simulation. At the first 10-ns production simulation, two harmonic restraints of 20 kcal/mol/Å^2 were added to keep the Mg^{2+} bound to the G10.1:N_7 and A9:O_{P2} positions. Another three harmonic restraints of 20 kcal/mol/Å^2 were used: the distances between G8:H_{OP2} and C1.1:O_{P5} and between G12:H_1 and C17:$O_{2'}$ were kept at around 1.8 Å to ensure initial hydrogen bonding, and the distance between A9:O_{P2} and C1.1:O_{P2} was kept at 4.3 Å (crystal distance). After 10 ns, all restraints were removed. The motions and relaxation of the solvent and counterions are notoriously slow to converge in nucleic acid simulations,[12] and careful equilibration is critical for reliable simulations. In summary, for each simulation, a total of 20 ns of equilibration (10 ns of solvent/ion relaxation and 10 ns of solvent and structure relaxation) was carried out and the production simulation was extended to 300 ns. Analysis was performed over the last 250 ns, with data collected every 10 ps.

Acknowledgements

T.-S.L. is grateful for financial support from the University of Minnesota through the Consortium for Bioinformatics and Computational Biology. We are grateful for the financial support provided by the National Institutes of Health (GM62248 to D.M.Y. and AI043393 to W.G.S.). G.M.G. is grateful for financial support from the University of Minnesota Training Program in Bioinformatics and Computational Biology. This work was supported, in part, by the University of Minnesota Biomedical Informatics and Computational Biology program (D.M.Y.) and by a generous allocation on an IBM Blue Gene BG/P with 4096 850-MHz CPUs at the IBM Advanced Client Technology Center in Rochester, MN. We further thank Cindy Mestad, Steven Westerbeck, and Geoffrey Costigan for technical assistance. Computational resources were provided in part by the Minnesota Supercomputing Institute.

Supplementary Data

Supplementary data associated with this article can be found, in the online version, at doi:10.1016/j.jmb.2009.02.054

References

1. Scott, W. G. (2007). Ribozymes. *Curr. Opin. Struct. Biol.* **13**, 280–286.
2. Scott, W. G. (1999). Biophysical and biochemical investigations of RNA catalysis in the hammerhead ribozyme. *Q. Rev. Biophys.* **32**, 241–294.
3. Martick, M. & Scott, W. G. (2006). Tertiary contacts distant from the active site prime a ribozyme for catalysis. *Cell*, **126**, 309–320.
4. Martick, M., Lee, T.-S., York, D. M. & Scott, W. G. (2008). Solvent structure and hammerhead ribozyme catalysis. *Chem. Biol.* **15**, 332–342.
5. Scott, W. G. (2007). Morphing the minimal and full-length hammerhead ribozymes: implications for the cleavage mechanism. *Biol. Chem.* **388**, 727–735.
6. Lee, T.-S., Silva-Lopez, C., Martick, M., Scott, W. G. & York, D. M. (2007). Insight into the role of Mg^{2+} in hammerhead ribozyme catalysis from X-ray crystallography and molecular dynamics simulation. *J. Chem. Theory Comput.* **3**, 325–327.
7. Lee, T.-S., Silva Lopez, C., Giambasu, G. M., Martick, M., Scott, W. G. & York, D. M. (2008). Role of Mg^{2+} in hammerhead ribozyme catalysis from molecular simulation. *J. Am. Chem. Soc.* **130**, 3053–3064.
8. Lee, T.-S. & York, D. M. (2008). Origin of mutational effects at the C3 and G8 positions on hammerhead ribozyme catalysis from molecular dynamics simulations. *J. Am. Chem. Soc.* **130**, 7168–7169.
9. Murray, J. B., Seyhan, A. A., Walter, N. G., Burke, J. M. & Scott, W. G. (1998). The hammerhead, hairpin and VS ribozymes are catalytically proficient in monovalent cations alone. *Chem. Biol.* **5**, 587–595.
10. O'Rear, J. L., Wang, S., Feig, A. L., Beigelman, L., Uhlenbeck, O. C. & Herschlag, D. (2001). Comparison of the hammerhead cleavage reactions stimulated by monovalent and divalent cations. *RNA*, **7**, 537–545.
11. Curtis, E. A. & Bartel, D. P. (2001). The hammerhead cleavage reaction in monovalent cations. *RNA*, **7**, 546–552.
12. Ponomarev, S. Y., Thayer, K. M. & Beveridge, D. L. (2004). Ion motions in molecular dynamics simulations on DNA. *Proc. Natl Acad. Sci. USA*, **101**, 14771–14775.
13. Wang, S., Karbstein, K., Peracchi, A., Beigelman, L. & Herschlag, D. (1999). Identification of the hammerhead ribozyme metal ion binding site responsible for rescue of the deleterious effect of a cleavage site phosphorothioate. *Biochemistry*, **38**, 14363–14378.
14. Suzumura, K., Takagi, Y., Orita, M. & Taira, K. (2004). NMR-based reappraisal of the coordination of a metal ion at the Pro$^-$ Rp oxygen of the A9/G10.1 site in a hammerhead ribozyme. *J. Am. Chem. Soc.* **126**, 15504–15511.
15. Torres, R. A. & Bruice, T. C. (2000). The mechanism of phosphodiester hydrolysis: near in-line attack conformations in the hammerhead ribozyme. *J. Am. Chem. Soc.* **122**, 781–791.
16. MacQueen, J. (1967). Some methods for classification and analysis of multivariate observations. In *Proceedings of the 5th Berkeley Symposium on Mathematical Statistics and Probability* (Le Cam, L. M. & Neyman, J., eds), vol. 1, pp. 281–297. University of California Press, Berkeley, CA, USA.
17. Davis, J. H., Foster, T. R., Tonelli, M. & Butcher, S. E. (2007). Role of metal ions in the tetraloop–receptor complex as analyzed by NMR. *RNA*, **13**, 76–86.
18. Vogt, M., Lahiri, S., Hoogstraten, C. G., Britt, D. R. & DeRose, V. J. (2006). Coordination environment of a site-bound metal ion in the hammerhead ribozyme determined by ^{15}N and ^{2}H ESEEM spectroscopy. *J. Am. Chem. Soc.* **128**, 16764–16770.
19. Persson, T. K., Hartmann, R. & Eckstein, F. (2002). Selection of hammerhead ribozyme variants with low Mg^{2+} requirement: importance of stem–loop II. *ChemBioChem*, **3**, 1066–1071.
20. Burke, D. H. & Greathouse, S. T. (2005). Low-magnesium, trans-cleavage activity by type III, tertiary stabilized hammerhead ribozymes with stem 1 discontinuities. *BMC Biochem.* **6**, 14.
21. Roychowdhury-Saha, M. & Burke, D. H. (2006). Extraordinary rates of transition metal ion-mediated ribozyme catalysis. *RNA*, **12**, 1846–1852.
22. Roychowdhury-Saha, M. & Burke, D. H. (2007). Distinct reaction pathway promoted by non-divalent-metal cations in a tertiary stabilized hammerhead ribozyme. *RNA*, **13**, 841–848.
23. Fedoruk-Wyszomirska, A., Szymanski, M., Wyszko, E., Barciszewska, M. Z. & Barciszewski, J. (2009). Highly active low magnesium hammerhead ribozyme. *J. Biochem.* E-pub ahead of print.
24. Nam, K., Gao, J. & York, D. M. (2008). Quantum mechanical/molecular mechanical simulation study of the mechanism of hairpin ribozyme catalysis. *J. Am. Chem. Soc.* **130**, 4680–4691.
25. Nam, K., Gao, J. & York, D. (2008). Electrostatic interactions in the hairpin ribozyme account for the majority of the rate acceleration without chemical participation by nucleobases. *RNA*, **14**, 1501–1507.
26. Smith, M. D., Mehdizadeh, R., Olive, J. E. & Collins, R. A. (2008). The ionic environment determines ribozyme cleavage rate by modulation of nucleobase pK_a. *RNA*, **14**, 1942–1949.
27. Humphrey, W., Dalke, A. & Schulten, K. (1996). VMD: Visual Molecular Dynamics. *J. Mol. Graphics*, **14**, 33–38.

28. Jorgensen, W. L., Chandrasekhar, J., Madura, J. D., Impey, R. W. & Klein, M. L. (1983). Comparison of simple potential functions for simulating liquid water. *J. Chem. Phys.* **79**, 926–935.
29. Phillips, J. C., Braun, R., Wang, W., Gumbart, J., Tajkhorshid, E., Villa, E. *et al.* (2005). Scalable molecular dynamics with NAMD. *J. Comput. Chem.* **26**, 1781–1802.
30. Cornell, W. D., Cieplak, P., Bayly, C. I., Gould, I. R., Ferguson, D. M., Spellmeyer, D. C. *et al.* (1995). A second generation force field for the simulation of proteins, nucleic acids and organic molecules. *J. Am. Chem. Soc.* **117**, 5179–5197.
31. Case, D. A., Pearlman, D. A., Caldwell, J. W., Cheatham, T. E., III, Wang, J., Ross, W. S. *et al.* (2002). *AMBER 7*. University of California San Francisco, San Francisco.
32. Pearlman, D. A., Case, D. A., Caldwell, J. W., Ross, W. R., Cheatham, T. E., III, DeBolt, S. *et al.* (1995). AMBER, a package of computer programs for applying molecular mechanics, normal mode analysis, molecular dynamics and free energy calculations to simulate the structure and energetic properties of molecules. *Comput. Phys. Commun.* **91**, 1–41.
33. Andersen, H. C. (1980). Molecular dynamics simulations at constant pressure and/or temperature. *J. Chem. Phys.* **72**, 2384–2393.
34. Nosé, S. & Klein, M. L. (1983). Constant pressure molecular dynamics for molecular systems. *Mol. Phys.* **50**, 1055–1076.
35. Hoover, W. G. (1985). Canonical dynamics: equilibration phase–space distributions. *Phys. Rev. A*, **31**, 1695–1697.
36. Essmann, U., Perera, L., Berkowitz, M. L., Darden, T., Hsing, L. & Pedersen, L. G. (1995). A smooth particle mesh Ewald method. *J. Chem. Phys.* **103**, 8577–8593.
37. Sagui, C. & Darden, T. A. (1999). Molecular dynamics simulations of biomolecules: long-range electrostatic effects. *Annu. Rev. Biophys. Biomol. Struct.* **28**, 155–179.
38. Allen, M. & Tildesley, D. (1987). *Computer Simulation of Liquids*. Oxford University Press, Oxford.
39. Ryckaert, J. P., Ciccotti, G. & Berendsen, H. J. C. (1977). Numerical integration of the Cartesian equations of motion of a system with constraints: molecular dynamics of *n*-alkanes. *J. Comput. Phys.* **23**, 327–341.